A Prototype DSN X/S-Band Feed: DSS 13 Application Status (Fourth Report)

W. Williams and H. Reilly
Radio Frequency and Microwave Subsystems Section

This article, the fourth in this series, discussing a prototype X/S-band common aperture horn feed for future use at various DSN sites and the Network Consolidation Program, deals with the final design and fabrication of the second-generation feedhorn and combiner. The results of the measurements obtained with the second-generation, full-scale feed configuration are presented.

I. Introduction

The first three articles (Refs. 1, 2, and 3) in this series discussed the development of a first-generation, dual-band (X-S) corrugated feedhorn for DSN applications. The earlier articles presented horn radiation patterns and resultant reflector antenna efficiencies using a half-scale horn model, the design of an X-S combiner permitting injection of both bands into the horn, and finally the measurements on the full-scale, first-generation horn and combiner.

The first horn model tests gave evidence of a small amount of "moding" in the X-band, but still within the specification requirement, and the X-S combiner had just enough S-band frequency bandwidth to satisfy the original narrow S-band requirement of approximately 40 MHz.

A second-generation horn system was begun and evolved where the major requirement was to increase the S-band performance across sufficient range to encompass DSN S-band high-power transmission as well as the DSN receive bands (2.10 to 2.30 GHz). As an adjunct, it was desired to determine the cause of X-band moding and, if possible, to correct it. The technique for broadening the combiner S-band bandwidth was by increasing the combiner radial line height and carefully designing a wideband matching network; the method of correcting X-band moding is discussed in Ref. 3.

II. The Full-Scale, Second-Generation X/S Horn

Early investigations into the causes of X-band moding indicated that the abrupt horn input angular change from cylindrical waveguide to the 34-degree wide-angle horn caused some moding, but probably not as much as noted. Therefore, the final horn version was to be built using a gradual change to the 34-degree flare angle over a 100-mm transition length to partially reduce moding.

A unique concept for this corrugated horn, relative to others that have been used, is the abrupt change in corrugation (groove) depth in the region of the horn where S-band is introduced. Grooves must be between ¼- and ½-wavelength deep to generate the proper corrugated waveguide hybrid mode. When cut the required depth for S-band, they become from 1¼- to 1½-wavelength deep in X-band, and hence will generate the proper X-band boundary conditions and modes.

However, the particular configuration of the combiner design in this program did not allow the full groove depths to be used in the horn input region where only X-band was present and so shallower grooves were used (¼ to ½ wavelength at X-band) at the input. This then necessitated an abrupt change near the combiner S-band input from the ¼-wavelength groove (X-band) to the 1¼ wavelength groove (X-band). This change represents a potential discontinuity in groove impedance for the X-band, dependent upon X-band frequency.

Experiments with sections of the first-generation horn revealed that this impedance discontinuity was the major cause of extraneous moding, (indicated by the level of cross polarization in the 45-degree pattern cut). Therefore, groove depths were cut that gave a groove impedance match near the center of the desired X-band range, and hence symmetrical mismatches at the band edges; e.g., at 7.8 GHz, the two groove depths at the abrupt change were 0.297λ (λ = X-band wavelengths) and 1.297λ, giving a "perfect" match. This resulted in measured -43-dB cross polarization, a good result indeed. At 7.1 GHz, the selected depth results in a 0.271λ input groove and a 1.18λ output groove, a mismatch giving rise to a cross-polarization level of -28 dB; however, this is still acceptable. At 8.45 GHz, the selected (7.8-GHz) depth results in a mismatch from 0.322λ to 1.405λ, and similar (-28-dB) cross-polarization levels.

Therefore, the full-scale, second-generation horn was made with X-band input grooves at 11.43 mm and output grooves at 49.89 mm, giving the ideal match at midband, 7.8 GHz, unfortunately a frequency region of no planned use. Our intentions are to provide 7.1-GHz and 8.4-GHz bands in the second-generation horn.

In the first-generation horn, the grooves were but 3.55-mm wide, the object being to have as many grooves per X-band wavelength as possible. This has always been reasonable in the past because such an assumption was made in theoretically solving for the hybrid mode fields in corrugated waveguide. However, in our second-generation horn (at the suggestion of B. M. Thomas, Ref. 4) the grooves were cut much wider; the only requirement being that they remain less than ½-wavelength wide at the highest intended frequency. This has worked quite well and permitted an easier (higher waveguide) access for the S-band horn input. The second generation horn has grooves of 12.7-mm width with a 3.55-mm wall.

The full-scale, second-generation horn was machined from five billets of aluminum with the smaller X-band input section and the X/S combiner made from separate pieces. The first generation horn exterior photograph given in Ref. 3 is not unlike our later development.

The radiation patterns of the second-generation horn have been measured at many frequencies throughout both the X and S bands. These measurements are made using linear polarizations. At each frequency, an E- and an H-plane pattern were recorded and also a pattern in the 45-degree plane. Also in the 45-degree plane the cross-polarization pattern was recorded, this indicating the lack or presence of unwanted radiating modes. E- and H-plane patterns are presented together on one graph while a second graph shows the 45-degree plane matched and cross polarized.

Figure 1 presents the results at X-band while Fig. 2 presents results at S-band. The E- and H-plane equivalence is very good and the complete lack of sidelobes down to minus 40 dB (and lower) contributes to a uniquely higher forward spillover efficiency than has been available before in X-band. Although the S-band patterns also are devoid of sidelobes, the shape of these patterns results in greater than typical forward spillover. Note the relative steepness on the sides of the X-band patterns compared to the sides of S-band patterns – a result of maintaining a sensible horn aperture size.

III. The Full-Scale, Second-Generation X/S Combiner

The first-generation X/S-band combiner performed its function well; it extracted the S-band receive signal from the horn at low loss, contributing little to system noise performance and its X-band isolation was great enough such that any additional X-band noise contribution was not detectable. However, this unit was, at S-band, of such narrow bandwidth that it could not be used for simultaneous S-band reception and transmission. Broadening the S-band bandwidth of this combiner so that receive/transmit functions could be included was the major objective of the second-generation development.

The first-generation combiner is comprised (see Ref. 2 for photos and a detailed discussion) of a thin radial line, only 8.89-mm wide, surrounding the horn at a horn diameter of about 119.4 mm and used to inject S-band into the horn. Internal to the radial line are a pair of X-band rejection chokes that isolated the X-band successfully so that no additional X-band noise could be detected as coming from the S-band portions. The very narrow radial line was chosen to help assure that no X-band energy could penetrate the combiner. However, this narrow line also tends to make the S-band passband more limited (as determined by the impedance variation with frequency looking into the combiner). The horn entry point (119.4-mm diam.) was selected for a best impedance match at 2.3 GHz and this resulted in a bandwidth of approximately 50 MHz over which input VSWR was less than 1.2:1.

In the second-generation combiner, the radial line section has been increased to 12.7 mm to increase the S-band bandwidth performance to include S-band transmission from 2.1 to 2.3 GHz. The band center is now lower (2.2 GHz) and therefore a new injection horn diameter of 127 mm is used. An increase to four X-band reject radial line chokes is used to maintain the required high X-band isolation. As with the first-generation combiner, tuning irises were required to be inserted into the radial line area to achieve an acceptable performance across the S-band. It was convenient to place these irises as metal blocks inserted into portions of the X-band chokes. A disassembled picture of this combiner is shown in Fig. 3.

The combiner along with its four 12.7-mm input waveguide terminals is not matched to standard S-band waveguide. The additional matching must be done with a transformer-tuner that transforms the 12.7-mm waveguide height to the 54.6-mm height of standard S-band (WR-430) waveguide and at the same time provides the necessary tuning to match the input impedance over the required bandwidth to a VSWR (voltage standing wave ratio) of less than 1.2:1. The graph shown in Fig. 4 represents the VSWR looking into any one of the four combiner input terminals. The requirement on the tuner is to develop a response VSWR of less than 1.2:1 from 2.1 to 2.3 GHz.

The transformer-tuner was designed and is fabricated using a 3-step, 2-section waveguide section to transform from the 12.7-mm height waveguide combiner input (standard 109.2-mm width), down to a narrow height guide of only 3.12 mm, increasing to a section of 39.4-mm height and then to the full 54.6 mm of standard waveguide. At the final step, an inductive iris is inserted into the 39.4-mm size that tunes the total combination across the required band. The VSWR response of the transformer-tuner and combiner is also shown in Fig. 4. Note that there exists a small region above 2.25 GHz where the VSWR exceeds 1.2:1, but this receive-only region is less critical than the lower or transmit end of the band, and fully acceptable.

The tuner-combiner is designed to transmit 20-kW CW power, or 5 kW into each tuner port under circular polarization excitation. Calculations of voltage breakdown in the 3.12-mm height section of waveguide indicate that it has this capability with sufficient safety factor. However, if the transmitter requirement should become 100 kW or more at a later date, there is serious question about the performance of this particular transformer-tuner design.

IV. A Tuner Design for High Power

Another model transformer-tuner was designed for the eventuality of higher power transmission. This unit has but two steps and one section to transform the required impedances. The minimum waveguide height of this unit is 12.3 mm and will withstand a 200-kW transmitter with sufficient safety factor. However, the unit does not meet the 1.2:1 VSWR specification across the entire 2.1- to 2.3-GHz S-band, but only in two narrow bands that include the present DSN transmit (2110- to 2120-MHz) and receive (2290- to 2300-MHz) bands. The VSWR response of the high-power tuner and combiner is also shown in Fig. 4. From Fig. 4, one notes that the two bands remain less than VSWR = 1.2 over roughly equal 35-MHz bandwidths.

V. Calculated Performance for DSS 13 Demonstration Application

Referring to Ref. 2, p. 41, one notes the discussion concerning the DSS 13 subreflector having been designed for S-band. Again, as in the first generation case, the measured horn patterns of Figs. 1 and 2 are used in a scattering program with the DSS 13 subreflector (including the vertex plate and outer flange) to determine the final primary reflector excitation and efficiency for the 26-meter paraboloid at DSS 13.

Two techniques are used to determine these subreflector scattered patterns. In one, the measured *far field* pattern is used to determine current excitations on the subreflector and finally the physical optics scattering. In the other technique, the horn radiation pattern is used to determine its spherical wave coefficients (Ref. 5) and these are then used to determine currents on the subreflector at its unique range from the horn, instead of assuming far field. These techniques agreed to within 0.5 percent, and so the far field approach is used for all calculations herein.

Figure 5 shows the DSS 13 scattered patterns in X-band and S-band. One can observe the effect of the S-band designed vertex plate at X-band with a smaller, perhaps modest, effect at S-band. Although subreflector blockage of radiated power is reduced to essentially zero at X-band, a corresponding X-band loss is noted (relative to S-band) in illumination efficiency and phase efficiency, due to pattern distortions related to the (oversized) vertex plate.

The efficiencies calculated from these scatter patterns are tabulated in Table 1. The 71.3-percent value at X-band is about 5 percent higher than the heretofore standard (22-dB) horn feed used, or about +0.3 dB.

Figure 6 presents the calculated far-field patterns from the 26-meter paraboloid. These patterns neglect the effect of spar blocking and surface tolerance; hence all final measured patterns will have somewhat higher sidelobes.

Using the geometrical shadow from the spars at DSS 13 and an empirically developed radio-frequency factor for spar blockage, a spar blockage efficiency of 0.861 has been determined. Also the surface tolerance (ϵ) at DSS 13 is less than 1.5-mm rms. When applied to the surface tolerance efficiency formula

$$\eta(\text{surface}) = \exp\left(\frac{-\{4\pi\epsilon\}^2}{\lambda}\right)$$

there results the surface tolerance efficiencies

75.4 percent at 8.450 GHz

97.9 percent at 2.295 GHz

The final expected performance at DSS 13 may now be obtained as shown in Table 2. These overall efficiencies neglect all feed internal losses and final feed VSWR.

VI. Conclusions

The X/S second-generation feed system will develop about 3-percent more gain than the standard 22-dB horn in the DSS 13 configuration. Also, since the noise contribution from rear spillover is less, a slight improvement in system noise temperature may be expected. A significant advantage will be seen in the application of this feed in other configurations, particularly the planned Network Consolidation Project. This will be the subject of a later article.

The concluding work on the horn system will take place at the DSN Microwave Test Facility where system noise and power capability will be measured. This will be the subject of a final article.

References

1. Williams, W. F., "A Prototype DSN X-S Band Feed: DSS 13 First Status Application," *DSN Progress Report 42-44, January and February 1978.* Jet Propulsion Laboratory, Pasadena, Calif.

2. Williams, W. F., "A Prototype DSN X-S Band Feed DSS 13 Application Status (Second Report)," *DSN Progress Report 42-47, July and August 1978.* Jet Propulsion Laboratory, Pasadena, Calif.

3. Williams, W., et al., "A Prototype DSN X/S Band Feed: DSS 13 Application Status (Third Report)," *DSN Progress Report 42-52, May and June 1979.* Jet Propulsion Laboratory, Pasadena, Calif.

4. Thomas, B. Mac A., "Design of Corrugated Horns," *IEEE Trans. on Ant. and Prop.*, Vol. AP-26, No. 2, March 1978.

5. Ludwig, Arthur C., "Near-Field Far-Field Transformations Using Spherical Wave Expansions," *IEEE Trans. on Ant. and Prop.*, Vol. AP-19, March 1971, pp. 214-220.

Table 1. Second-generation DSS 13 efficiencies

Efficiency	Frequency = 8.450 GHz	Frequency = 2.290 GHz
Rear spillover	0.997	0.994
Forward spillover	0.979	0.889
Illumination	0.811	0.865
Cross-polarization	0.999	0.999
Phase	0.902	0.925
Blockage (subreflector)	1.0	0.972
Total	0.713	0.686

Table 2. Second-generation DSS 13 final overall efficiency

Efficiency	Frequency = 8.450 GHz	Frequency = 2.295 GHz
RF feed efficiency	0.713	0.686
Surface efficiency	0.754	0.979
Spar blockage	0.861	0.861
Final overall efficiency	0.463	0.578

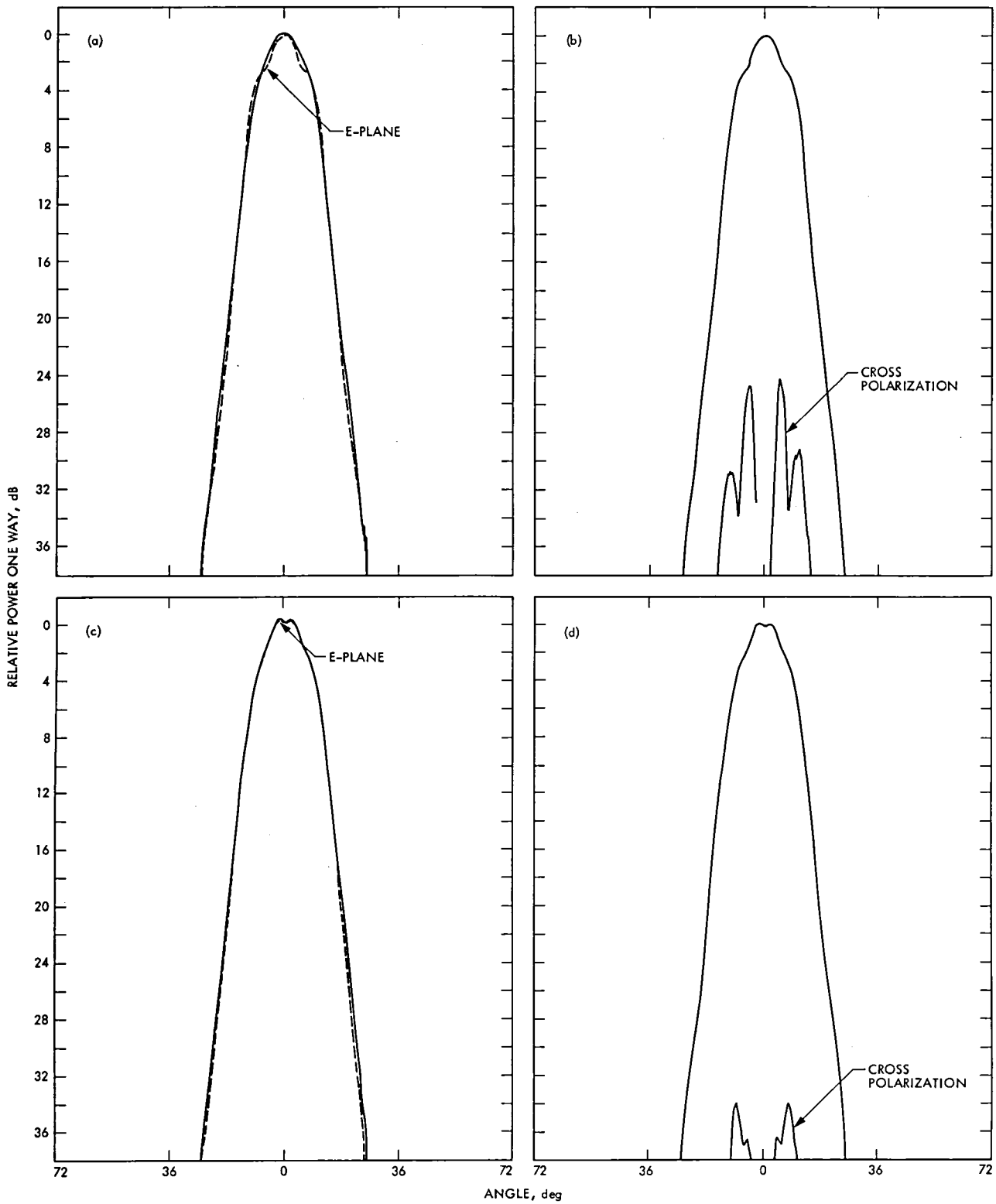

Fig. 1. Radiation patterns of the second-generation feedhorn in X-band: (a) E and H plane patterns at 8.45 GHz; (b) pattern cut at 45 deg to show cross polarization at 8.45 GHz; (c) E and H plane patterns at 7.8 GHz; (d) pattern cut at 45 deg to show cross polarization at 7.8 GHz; (e) E and H plane patterns at 7.1 GHz; (f) pattern cut at 45 deg to show cross polarization at 7.1 GHz

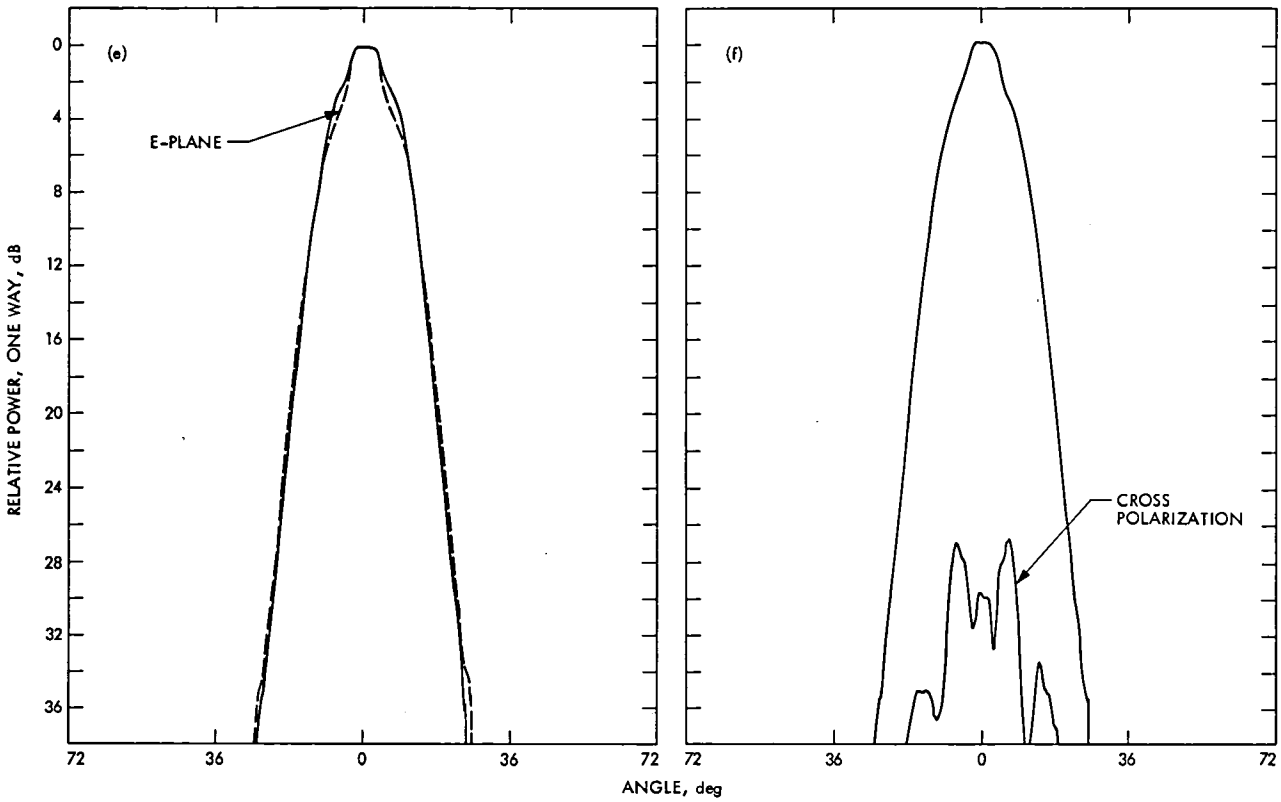
(e)
(f)
E-PLANE
CROSS POLARIZATION
RELATIVE POWER, ONE WAY, dB
0
4
8
12
16
20
24
28
32
36
72
36
0
36
72
ANGLE, deg

Fig. 1 (contd)

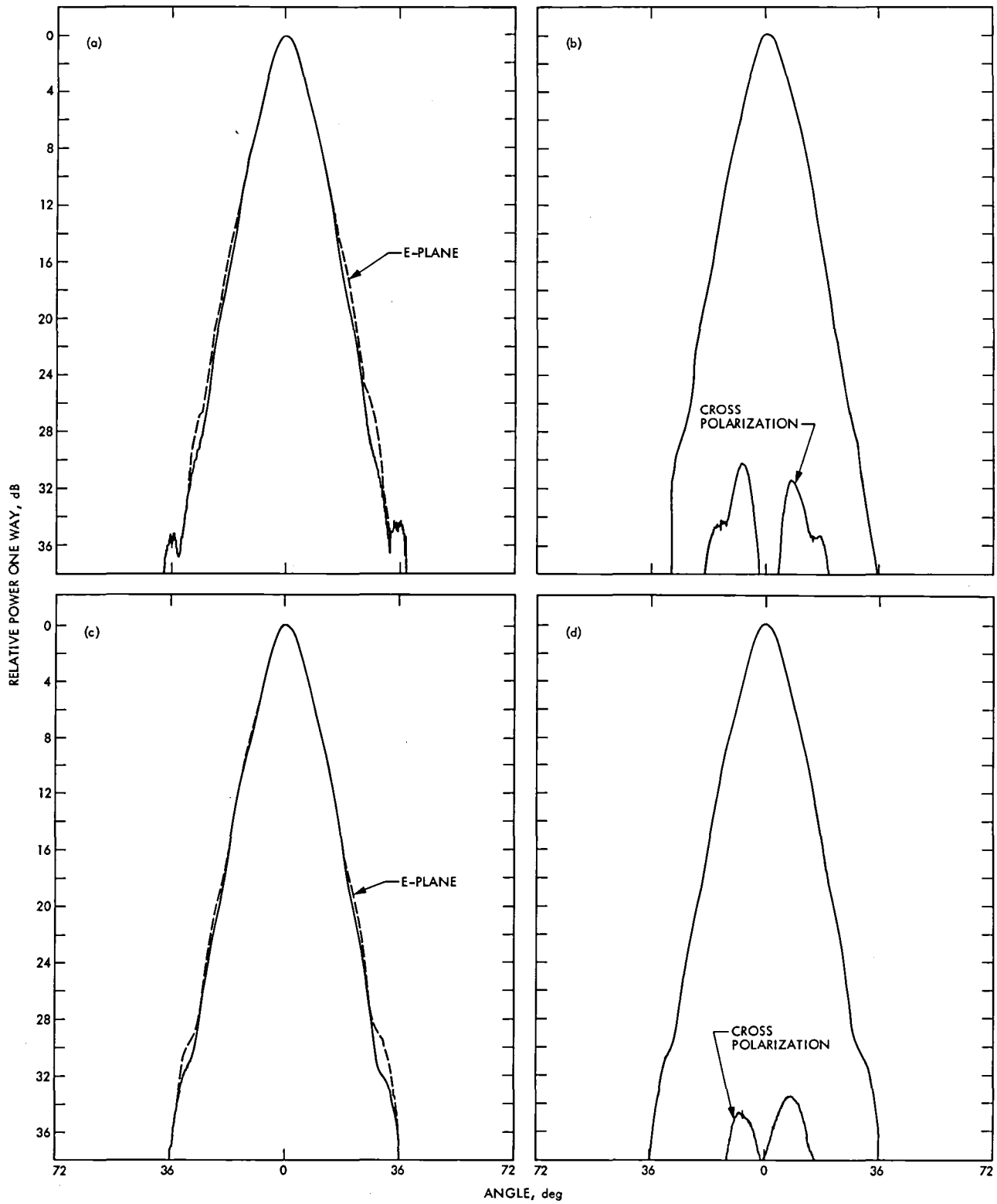

Fig. 2. Radiation patterns of the second-generation feedhorn in S-band: (a) E and H plane patterns at 2.3 GHz; (b) pattern cut at 45 deg to show cross polarization at 2.3 GHz; (c) E and H plane patterns at 2.1 GHz; (d) pattern cut at 45 deg to show cross polarization at 2.1 GHz

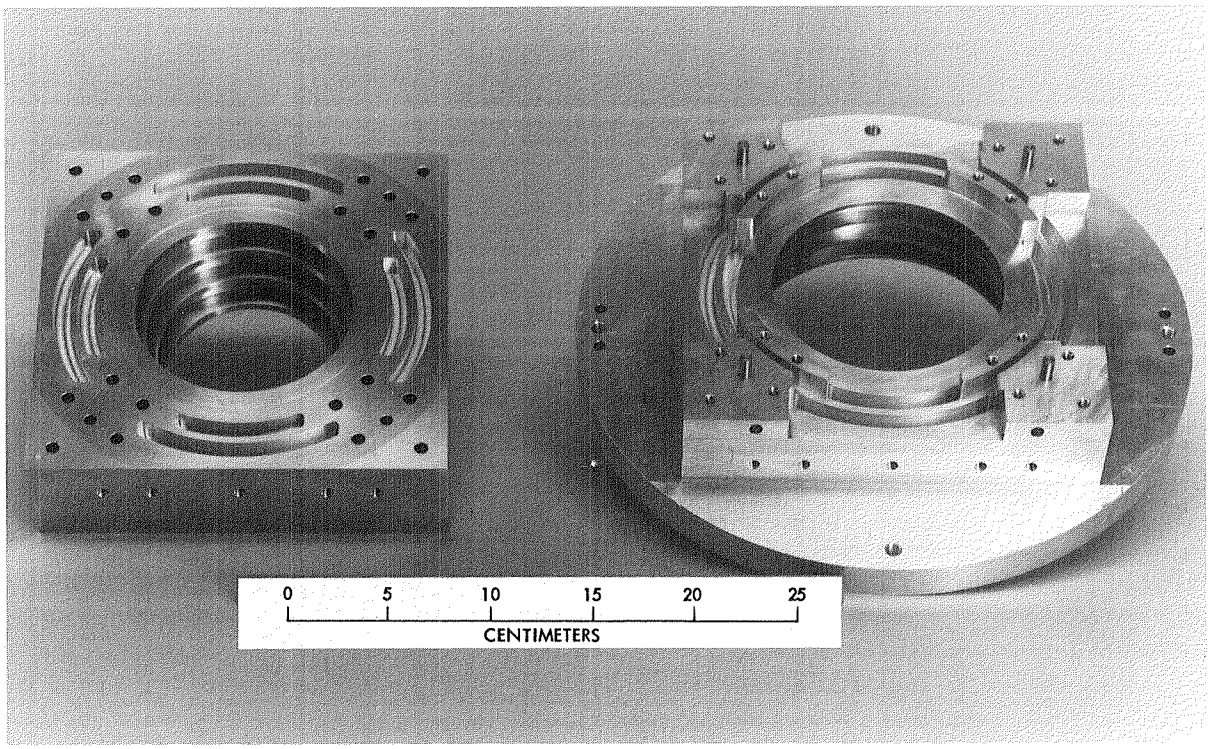

Fig. 3. The Mod II X/S Combiner

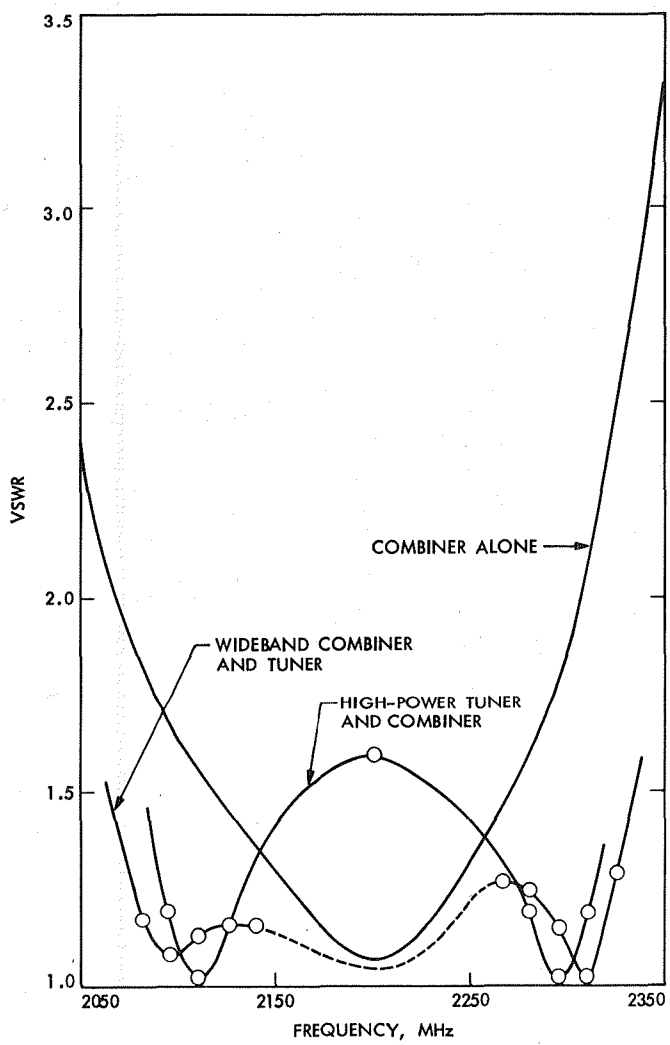

Fig. 4. The VSWR at input to the second-generation combiner and at the tuner input

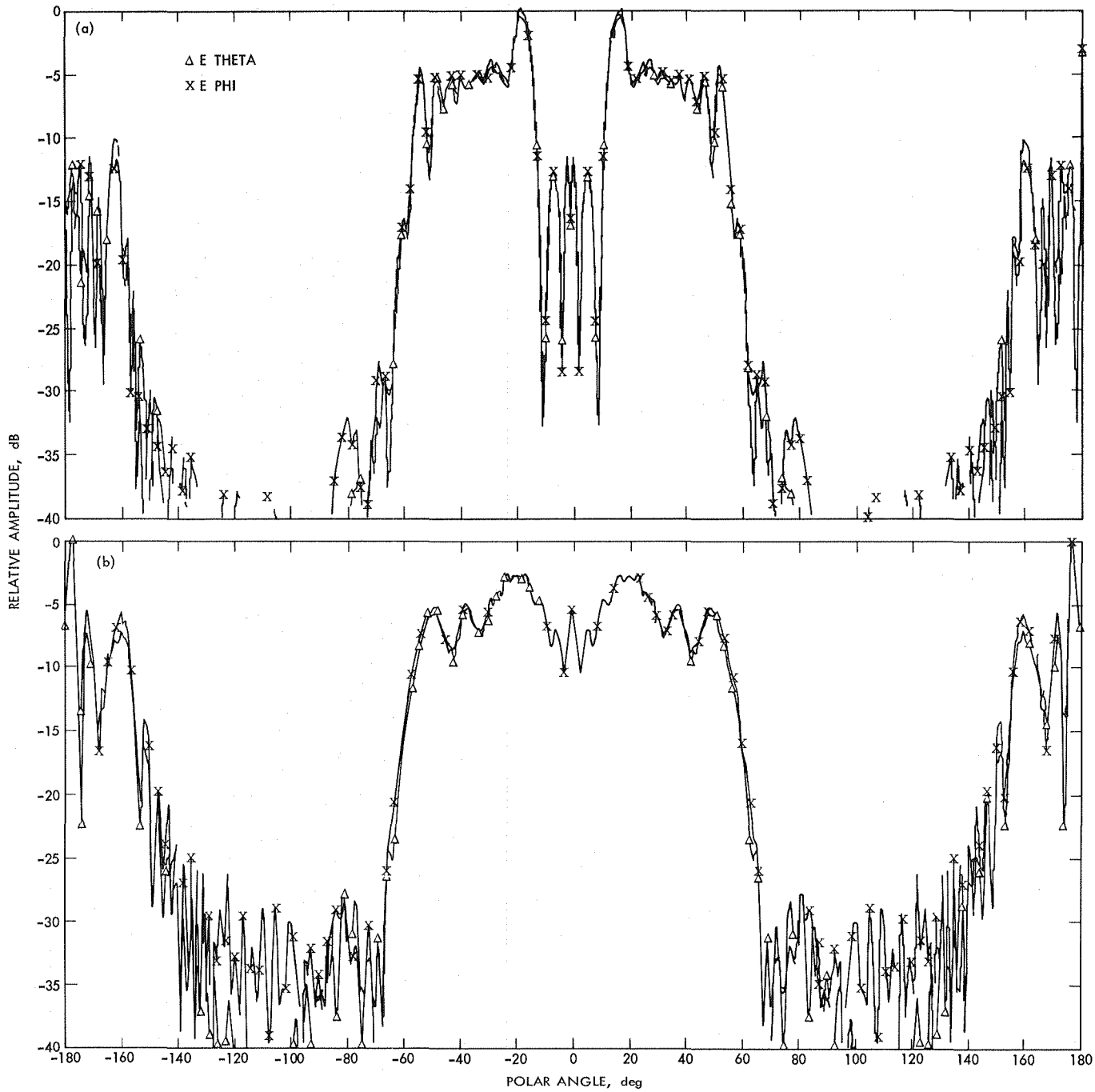

Fig. 5. Subreflector scattering at azimuth angle = 0.00, second-generation horn from the DSS 13 subreflector: (a) at 8.450 GHz; (b) at 2.295 GHz

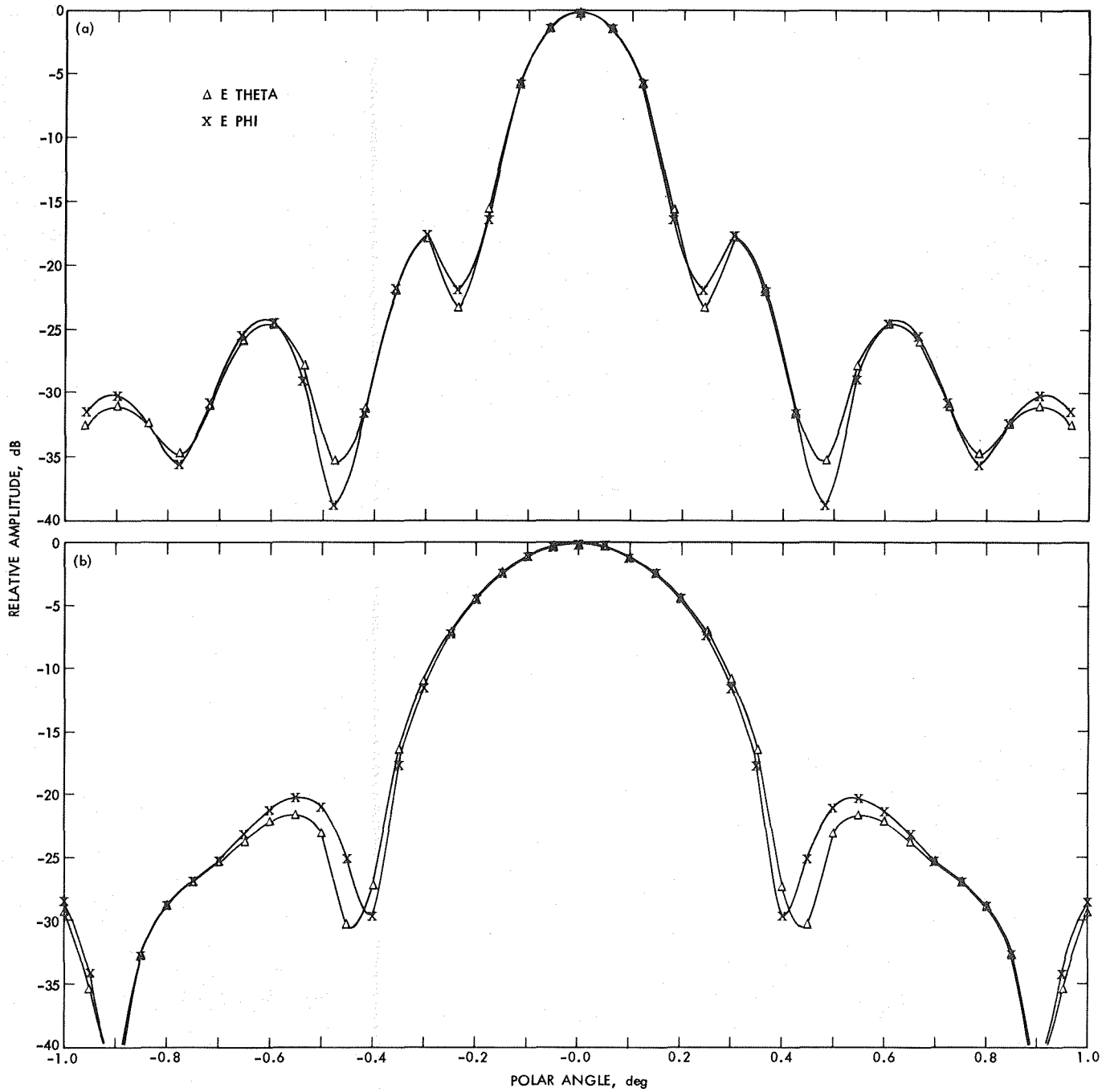

Fig. 6. Secondary patterns at azimuth angle = 0.00 from the Venus paraboloid (DSS 13): (a) at 8.450 GHz; (b) at 2.295 GHz